Pharmaceutical Research, Vol. 25, No. 10, October 2008 (© 2008)
DOI: 10.1007/s11095-008-9615-2

Research Paper

Solid Lipid Nanoparticles Enhance the Delivery of the HIV Protease Inhibitor, Atazanavir, by a Human Brain Endothelial Cell Line

Niladri Chattopadhyay,[1] Jason Zastre,[1] Ho-Lun Wong,[1] Xiao Yu Wu,[1] and Reina Bendayan[1,2]

Received February 28, 2008; accepted April 28, 2008; published online May 31, 2008

Purpose. Protease inhibitors (PIs) exhibit low brain permeability. As a result, unchallenged HIV viral replication can lead to HIV-encephalitis and antiretroviral drug resistance. The objective of this study was to develop and evaluate a lipid nanoparticle system for enhanced brain delivery of the potent and frequently used HIV PI, atazanavir, using a well characterized human brain microvessel endothelial cell line (hCMEC/D3) representative of the blood-brain barrier.
Methods. Solid lipid nanoparticles (SLNs) were prepared by a thin film hydration technique and analyzed for atazanavir encapsulation efficiency, particle size, morphology, zeta potential and drug release. Cell viability experiments demonstrate that SLNs exhibit no toxicity in hCMEC/D3 cells up to a concentration corresponding to 200 nM of atazanavir.
Results. Spherical SLNs with an average particle size of ~167 nm were formulated. Delivery of [^{3}H]-atazanavir by SLNs led to a significantly higher accumulation by the endothelial cell monolayer as compared to the drug aqueous solution. Furthermore, release of Rhodamine-123 (a fluorescent probe) by SLNs also resulted in a higher cellular accumulation.
Conclusions. These data suggest that SLNs could be a promising drug delivery system to enhance brain uptake of atazanavir and potentially other PIs.

KEY WORDS: atazanavir; drug delivery; hCMEC/D3 human brain microvessel endothelial cells; HIV-protease inhibitor; solid lipid nanoparticles.

INTRODUCTION

Since the introduction in 1987 of the nucleoside reverse transcriptase inhibitor zidovudine for the treatment of human immunodeficiency virus (HIV) infection, intensive efforts have resulted in the discovery of several classes of antiviral drugs including nucleoside reverse transcriptase inhibitors, non-nucleoside reverse transcriptase inhibitors, protease inhibitors (PIs), fusion inhibitors and integrase inhibitors. Despite the *in vitro* efficacy of antiretroviral drugs, pharmacological treatment is compromised by its inherent physico-chemical properties and limitations in bio-distribution and cellular uptake (1). For example, in HIV viral reservoirs such as the central nervous system (CNS), effective drug availability is impeded by restricted antiretroviral drug transport across the blood-brain barrier (BBB) (2,3).

PIs have dramatically influenced the outcome of HIV infection in the periphery. However, they have limited ability to reach the CNS, with the majority of this class of drugs not detected in human cerebrospinal fluid (3). It has been suggested that the high lipophilicity, high molecular weight (>500 Da) as well as the presence of numerous amide bonds in these compounds result in less desirable physico-chemical properties. In addition, active efflux by ATP binding cassette membrane associated-transporters can dramatically limit their brain permeability.

Drug delivery to the CNS poses a formidable challenge. Two major barriers, the BBB and the blood-cerebrospinal fluid barrier can hamper effective transport of drugs into the brain. Several drug delivery systems, including immunoliposomes (4), polymeric nanoparticles (5), and lipid nanoparticles (6) have been assessed for their ability to transport and deliver drugs across the BBB. Due to their small size range, nanoparticle systems have been proposed as potential brain targeting systems (7). Nanoparticle drug delivery systems have been increasingly used to improve the efficiency of antiretroviral drugs with most of the work being focused on enhancing the delivery of saquinavir (8–13). In particular, Bender *et al.* (12) reported the encapsulation of saquinavir *via* emulsion polymerization in polyhexylcyanoacrylate nanoparticles. These investigators found that in contrast to an aqueous solution, saquinavir delivered by nanoparticles elicited important improvement in antiviral activity in both chronic and acute infection, *in vitro*. Recently, Shah and Amiji (14) reported the enhanced uptake of saquinavir in a THP-1 human monocyte/macrophage cell line, when saquinavir was delivered by a poly(ethylene oxide)-modified poly (epsilon-caprolactone) nanoparticulate system. Several studies have evaluated the ability of SLNs to increase brain drug concentration *in vivo* (15–20). Koziara *et al.* ((21) have

[1] Department of Pharmaceutical Sciences, Leslie Dan Faculty of Pharmacy, University of Toronto, Ontario, Canada M5S 3M2.
[2] To whom correspondence should be addressed. (e-mail: r.bendayan@utoronto.ca)

developed lipid nanoparticles comprised of emulsifying wax and Brij 72 for CNS delivery of paclitaxel. Brain uptake of paclitaxel as assessed by *in situ* perfusion studies was significantly enhanced when paclitaxel was encapsulated in nanoparticles. The authors hypothesized that paclitaxel loaded nanoparticles could mask some of the drug transport characteristics and thus limit its binding to efflux transporters such as P-glycoprotein (P-gp), which consequently would lead to higher brain and tumor cell uptake of the otherwise effluxed drug. Furthermore, Lockman *et al.* (22) have demonstrated the potential of enhancing drug delivery to the brain by using thiamine coated lipid nanoparticles. Finally, it has been reported that Poly(alkyl cyanoacrylate) nanoparticles coated with surfactants such as Pluronic® F68 and Polysorbate 20, 40, 60 or 80 can be transported across the BBB (23). These authors suggest that the most likely route of transport of the nanoparticles across the BBB occurs *via* receptor mediated endocytosis. It has been demonstrated that surfactant coated nanoparticles preferentially adsorb apolipoprotein E and/or B from the bloodstream (23) and mimic lipoprotein particles which are then potentially endocytosed by the low-density lipoprotein (LDL) receptors present on the endothelial cells lining the brain blood capillaries. The drug from the nanoparticles may then, be released either within these cells followed by passive diffusion into brain parenchyma or can be transported into the brain by transcytosis. Recent work by Ryoung *et al.* (24) supports the LDL receptor mediated hypothesis.

Atazanavir Sulphate (Reyataz®, Bristol Meyer Squibbs, MW: 802.9 g/mol) is an azapeptide inhibitor of HIV-1 protease frequently used in the treatment of HIV infection. It is a potent PI with a mean 50% effective concentration (EC50) in the absence of human serum of 2 to 5 nM against a variety of laboratory and clinical HIV-1 isolates grown in peripheral blood mononuclear cells, macrophages, CEM-SS cells, and MT-2 cells. Atazanavir is highly selective for HIV-1 protease and exerts protease enzyme inhibition associated cytotoxicity at concentrations 6,500- to 23,000-fold higher than those required for therapeutic antiviral activity (25,26). It is also reported to exhibit a 2- to 20-fold higher antiretroviral activity compared to other PIs (27). Thus, due to its superior clinical profile, lower toxicity and frequent use, atazanavir is an attractive candidate for encapsulation in a nanoparticle drug delivery system for brain targeting.

Since, it has been suggested that HIV PIs may completely associate with lipid nanoparticles (9), we hypothesized that SLNs, with their lipid core and shell, may be an appropriate delivery vehicle for atazanavir encapsulation. The objective of this study was to develop and evaluate a lipid nanoparticle system for enhanced brain delivery of atazanavir, using a well characterized human brain microvessel endothelial cell line (hCMEC/D3) representative of the BBB.

MATERIALS AND METHODS

Materials

Atazanavir sulphate, was extracted using methanol from commercially available capsules (Reyataz®, Bristol Myers Squibb, NJ, USA). Stearic acid was purchased from Sigma Aldrich, (Mississauga, Ontario, Canada). National Formulary grade Pluronic®F-68 was a gift from BASF Inc., (Parsippany, NJ, USA). [^{3}H]-atazanavir (specific activity of 3 Ci/mmol) was custom tritiated by Moravek Biochemicals (Brea, CA, USA). Rhodamine-123 was obtained from Molecular Probes (Eugene, OR, USA). Atazanavir standard reference was kindly provided by the National Institutes of Health AIDS Research and Reference Reagent Program, Division of AIDS, National Institute of Allergy and Infectious Diseases, National Institutes of Health (Bethesda, MD, USA). Deionized distilled water (Millipore, MA, USA) was used to prepare aqueous solutions. All other reagents were purchased from Sigma Chemicals (Mississauga, Ontario, Canada) and were of the highest available purity.

Extraction of Atazanavir

Methanol was used as an extracting solvent since the formulation excipients crospovidone, lactose monohydrate, and magnesium stearate have poor solubility in methanol (28). The extracted atazanavir was compared to a standard obtained from the National Institutes of Health AIDS Research and Reference Reagent Program, Division of AIDS, National Institute of Allergy and Infectious Diseases, National Institutes of Health (Bethesda, MD) at a concentration of 50 μg/ml using a UV spectrophotometer (Agilent 8453 UV spectrophotometer, Germany).

Preparation of Atazanavir Loaded Solid Lipid Nanoparticles (SLNS)

Atazanavir loaded SLNs were formulated by a thin film hydration technique using a microemulsion technique as previously described (29). Stearic acid (25 mg) was dissolved in 1 ml of 3% *w*/*w* Pluronic®F68 aqueous solution. Atazanavir, dissolved in methanol (1.25 mg for a total drug loading of 5% *w*/*w*), was added to the lipid-surfactant solution. The resulting mixture of atazanavir, stearic acid and Pluronic®F68 was then stirred for approximately 30 min. The organic solvents were then evaporated under nitrogen to form a thin lipid film and the dried film was subsequently treated with 0.5 ml of deionized water maintained at approximately 80–82°C. The resultant emulsion was then subjected to alternate cycles of heat and vortexing for 5 min to facilitate rapid formation of a microemulsion (21). Once a clear phase was obtained, the microemulsion was ultrasonicated with intermittent periods of vortexing for 3 min to further reduce the particle size. SLN containing atazanavir were formed by dispersing the microemulsion in 4.5 ml of deionised water maintained at 2–4°C.

Characterization of Atazanavir Loaded SLNS

Drug Loading and Encapsulation Efficiency

Maximum atazanavir loading into SLNs was determined by adding increasing amounts of atazanavir (1, 2, 5, 7.5, 10 and 20%). Encapsulation efficiency of atazanavir in SLNs was determined by centrifugal filtration using an ultrafiltration membrane. Briefly, 1.5 ml of the freshly prepared atazanavir loaded SLNs were placed in the filter unit of a 5,000 MW cut

off centrifugal filter device (Amicon® Ultra-4, Millipore, USA). Since the filter devices contain trace amounts of glycerine, they were pre-rinsed with deionized water. The device was centrifuged at 2,000×*g* to obtain an ultrafiltrate. The amount of unencapsulated atazanavir present in the ultrafiltrate was measured by UV spectrophotometry (Agilent 8453 UV spectrophotometer, Germany) at 249 nm. The concentration was obtained from a standard curve of atazanavir prepared in deionized distilled water. To account for any loss of atazanavir due to adsorption onto the ultrafiltration membrane, the adsorption of atazanavir on the membrane was evaluated by separate filtration studies of aqueous solutions of atazanavir at equivalent drug loading concentrations. The amount of drug loading and encapsulation efficiency was calculated based on the amount of free drug measured using the following equations:

$$Drug\ Loading\ (\%) = \frac{W_a - W_s}{W_a - W_s + Wl} \tag{1.1}$$

W_a Amount of drug added to the formulation
W_s Amount of unencapsulated drug measured in the ultrafiltrate
W_l Weight of the lipid

$$Encapsulation\ efficiency\ (\%) = \frac{W_a - W_s}{W_a} \tag{1.2}$$

Particle Size Analysis

The average diameter of SLNs was measured using an instrument combining the function of photon correlation spectroscopy (PCS) and zeta potential measurement (Nicomp Zetasizer 380, USA), at a fixed angle of 90° using a He–Ne laser at 633 nm. The parameters of the particle size analyzer were set as follows: temperature at 23°C, viscosity at 0.933 cp, and index of refraction at 1.333. Each SLN sample was diluted 1:50 with deionized, 0.22 μm filtered water (Millipore, USA) until a count rate of 200–300 kHz was achieved. Volume-weighted gaussian analysis was used for reporting particle size distribution. Particle size was determined using two 5-min cycles for each sample, and each value reported is the average of five measurements.

Zeta Potential

Zeta potential is a key factor to evaluate the stability of a colloidal dispersion (30), and the surface charge on the particle was determined using a Nicomp Zetasizer 380 instrument (Particle Sizing Systems, USA) at a fixed angle of 19° and platinum electrodes. A typical sample was prepared by diluting the SLNs with 0.1% Pluronic®F68 aqueous solution. The sample was placed in 4.5 ml, 10 mm pathlength polystyrene cuvets (Fisher Scientific, USA). The zeta potential reported is the average of three independent formulations.

Transmission and Scanning Electron Microscopy (TEM/SEM)

The morphology of blank and atazanavir loaded nanoparticles was examined by TEM (Hitachi 7000H, Japan). Nanoparticles were stained with phosphotungstic acid and passively adsorbed onto a 500 mesh carbon-coated copper grid. Excessive stain was removed by a Whatman No. 1 filter paper. For SEM analysis, atazanavir loaded SLNs were mounted on conductive carbon adhesive attached to aluminium stubs. The sample was then coated with gold (5 nm thick layer) in a Polaron SC7640 sputter coater (Quorum Technologies, Sussex, UK) for 100 s. The sample was viewed with a Hitachi S 570 scanning electron microscope (Hitachi, Japan), using a secondary electron detector with accelerating voltage of 15 kV and a working distance of 2 mm. Images for both TEM and SEM were digitally captured using Quartz PCI digital imaging software (Quartz Imaging Corporation, British Columbia, Canada).

Drug Release

Atazanavir release from the SLNs was determined by a dialysis bag method using a 15,000 molecular weight cut off membrane and phosphate-buffered saline (PBS) (pH 7.4, 37°C) as the release medium. Atazanavir loaded SLNs were prepared as described previously. Five ml of the formulation was placed in the dialysis tubing [pre-equilibrated in PBS (pH 7.4, 37°C) for 30 min] and both ends of the bag were clamped. The bag containing the formulation was placed in the release medium and stirred using a magnetic stirrer. The drug released into the medium was assayed every 10 min over a period of 24 h using a UV spectrophotometer (λ=249 nm). The amount of drug released was calculated from a standard curve of atazanavir in PBS (pH 7.4, 10 mM).

Cell Culture

hCMEC/D3 is an immortalized human brain microvessel endothelial cell line kindly provided by Dr. Couraud (Institut Cochin, Paris, France). The cell line was isolated from normal human brain endothelial cells transduced by lentiviral vectors incorporating human telomerase, to prolong the stable life span of differentiated cells in culture, and SV40 T antigen, to promote proliferation. Normal human brain tissue was obtained following surgical excision of an area from the temporal lobe of an adult female with epilepsy. The hCMEC/D3 cell line is an extensively characterized human brain endothelial cell line, which mimics most of the key characteristics of the BBB, even in the absence of co-cultured glial cells. It is a useful model for screening CNS drug candidates, as well as for drug delivery systems to the brain (23). In the present studies, hCMEC/D3 cells (Passage 33–44) were grown as a monolayer on 75 cm^2 polystyrene cell culture flasks and 6 or 96 well plates (Sarstedt, St. Leonard, Quebec, Canada). Prior to plating, all the flasks were coated with Type I rat tail collagen (Sigma-Aldrich). All cultures were maintained at 37°C in an atmosphere of 95% air and 5% CO_2. The culture medium was replaced on alternate days until the cells reached ~90% confluency. Confluent cultures were harvested by washing the cells with PBS. The cells were then detached with a 0.25% trypsin/EDTA solution for 3 min followed by reseeding in collagen-coated flasks.

Cell Viability

Viability of hCMEC/D3 cells in the presence or absence of free atazanavir, blank as well as atazanavir loaded SLNs over a period of 24 h was evaluated by a 3-[4,5-dimethylthiazol-2-yl]-2,5-diphenyl-tetrazoliumbromide (MTT) assay as previously described (31,32). Cell viability in the presence of the various treatments was calculated as a percent of control cells.

Preparation of [^{3}H]-Atazanavir-Loaded SLNS

Atazanavir was custom tritiated by Moravek biochemicals (Brea, CA, USA) at a concentration of 3 Ci/mmol. Tritiated [^{3}H]-saquinavir loaded nanoparticles were prepared by mixing 15 μl of radioactive atazanavir with 238 μg of non-radioactive atazanavir and 5 mg of stearic acid following the procedure as described for non-radioactive SLNs. The encapsulation efficiency of [^{3}H]-atazanavir in SLNs was evaluated by a ultrafiltration technique using a 10 kDa centrifugal filter device with a regenerated cellulose membrane (Microcon YM-10, Millipore, MA, USA). An aliquot of 500 μl of the formulation was added to the sample reservoir and centrifuged at 8,000 rpm for 20 min. Then 100 μl of the obtained filtrate was mixed with 2 ml of Pico-Fluor (PerkinElmer, Massachusetts, USA) and analysed for unencapsulated [^{3}H]-atazanavir using a liquid scintillation counter (Beckman LS5000 TD, Beckman Coulter, Inc., California, USA). Encapsulation efficiency was calculated as per Eq. 1.2.

Uptake Studies

Drug uptake of [^{3}H]-atazanavir loaded SLNs, or blank SLNs in the presence of [^{3}H]-atazanavir aqueous solution, or [^{3}H]-atazanavir aqueous solution prepared in Hank's buffered salt solution (HBSS) was evaluated in confluent hCMEC/D3 monolayer cells. Cells were washed three times with HBSS (pH 7.4, 37°C, 10 mM HEPES) and pre-equilibrated in HBSS for 30 min. After the equilibration period, HBSS was removed and replaced with the above mentioned treatments at 37°C for 15, 60, or 120 min. All treatments were adjusted to a concentration of 200 nM of atazanavir. After each incubation, the medium was removed and the uptake process was stopped by washing the cells three times with ice-cold PBS (pH 7.4). The cells were then trypsinized with trypsin/EDTA, and solubilized with 1% Triton-X. The solubilized cells were then transferred to polyethylene scintillation vials (VWR, Ontario, Canada) with further addition of scintillation cocktail (Pico-Fluor, PerkinElmer). The amount of cellular drug uptake was measured using a liquid scintillation counter (Beckman LS5000 TD, Beckman Coulter, Inc.). Accumulation of [^{3}H]-atazanavir was standardized to the cellular protein concentration (mg ml^{-1}) determined by the Bradford colorimetric method (26) using bovine serum albumin (Sigma- Aldrich) as the standard. The amount of drug uptake was expressed as (pmol mg^{-1}) of protein.

Fluorescence Microscopy

Rhodamine 123 (R123) was used as a hydrophobic fluorescence probe to compare cellular uptake of R123 loaded SLNs to the uptake of an aqueous solution of R123. R123 loaded SLNs with a maximum drug loading of 0.7% *w*/*w* were prepared similar to atazanavir loaded SLNs. Treatment of monolayer cells with R123 loaded SLNs ensured that the unencapsulated R123 was removed by ultrafiltration and then adjusted to 53.3 μg/ml of SLNs equivalent to approximately 1 μM of R123. Control treatment (aqueous R123) was adjusted to 1 μM as well. hCMEC/D3 cells were grown as a monolayer on sterile glass coverslips and maintained at 37°C, 5% CO_2/95% air. On the day of the experiment, confluent cells were washed three times with HBSS (pH 7.4, 10 mM HEPES) and pre-equilibrated in HBSS for 30 min. After the pre-equilibration period, the HBSS was removed and replaced with R123 loaded SLNs diluted in HBSS or R123 prepared in HBSS. The cells were then incubated for 2 h. At the end of the incubation period, cells were washed three times with ice-cold PBS and examined at 40× magnification with an exposure time of 3 s using a Nikon Eclipse E1000R fluorescent microscope (Nikon, Tokyo, Japan). Images were acquired with the SimplePCI imaging software (Compix Inc., Imaging Systems, Pennsylvania, USA).

Statistical Analysis

Statistical analysis was performed on the extent of cellular drug uptake upon treatment with (1) [^{3}H]-atazanavir-SLNs, (2) blank SLNs in the presence of [^{3}H]-atazanavir aqueous solution and (3) [^{3}H]-atazanavir aqueous solution using one-way analysis of variance with post-hoc Bonferroni analysis with the aid of a computer statistical program [Statistical Package for the Social Sciences (SPSS), Version 14.0, SPSS Inc, Chicago, USA]. Results are reported as a mean±SD from a minimum of three independent experiments performed in monolayer cells pertaining to different passages. Differences were considered significant at $p \leq 0.05$.

RESULTS

Atazanavir Extraction and Comparison with NIH Standard Reference, Drug Loading and Encapsulation Efficiency

Atazanavir can be easily purified from commercially available capsules using methanol extraction. The extracted atazanavir was compared to a standard obtained from the National Institutes of Health. Sparidans *et al.* (27) have reported peaks of atazanavir at 250 and 280 nm respectively. We identified two peaks at 249 and 281 nm respectively, for both extracted and standard Atazanavir (data not shown).

Maximum atazanavir loading was determined by adding various amounts of the drug (1, 2, 5, 7.5, 10 and 20% *w*/*w* of stearic acid) and measuring the encapsulation efficiency. The formulations were observed visually for precipitation. There was no detectable atazanavir or R123 loss by adsorption onto the filtration membrane and therefore no adjustments were made in the calculation of their encapsulation. Table I shows the extent of atazanavir encapsulation in the SLNs with an increasing drug load. Atazanavir has a high encapsulation efficiency of approximately 90% at a satisfactory drug load of 5% *w*/*w* of the lipid. The encapsulation efficiency decreased from approximately 99% for a 1% *w*/*w* load to approximately 90% for a 5% load. The encapsulation efficiency of atazana-

Table I. Encapsulation Efficiency, Particle Size and Zeta Potential of Atazanavir Loaded SLNs

	Encapsulation Efficiency (%)	Average Particle Size (nm)	Polydispersity Index	Zeta Potential (mV)
Drug loading % *w/w*				
1	98.9+0.8			
2	98.2+1.3			
5	89.3+2.7			
Day(s)				
Day 0		167±8.3	0.16±0.04	−18.43±0.70
Day 3		215±34.5	0.17±0.04	
Day 7		224.5±7.7	0.31±0.10	

vir (using [^{3}H]-atazanavir as tracer), as determined using liquid scintillation counting, was approximately ~93%. For R123, a maximum load of 0.7% w/w could be achieved with encapsulation efficiency in SLNs of ~71%.

Particle Size Analysis

The mean particle size and size distribution of atazanavir-loaded SLNs were assessed by dynamic light scattering. The particle size of the atazanavir-loaded SLNs was evaluated 1 h after preparation and after storage at 4°C on days 3 and 7 respectively. Freshly prepared blank and atazanavir-loaded SLNs were also analyzed for particle size using TEM. The mean particle size of a freshly prepared sample as determined by dynamic light scattering was ~167 nm (Table I). The average particle size of a sample stored at 4°C increased to ~215 and ~224 nm on the third and seventh day respectively. The average particle size of SLNs in the TEM image field for blank SLNs (Fig. 1A) was approximately 110 nm and the average particle size for atazanavir-loaded SLNs (Fig. 1B) in the TEM field was approximately 156 nm. Additionally, as seen in Fig. 1C, SEM micrographs of atazanavir-loaded SLNs suggest that the particles have a uniform spherical shape with a smooth surface.

Zeta Potential

Zeta potential is a key factor to evaluate the stability of a colloidal dispersion (30) and the surface charge on atazanavir-loaded SLNs was determined using a Nicomp Zetasizer 380 instrument (Particle Sizing Systems, USA) by diluting the SLN with 0.1% Pluronic®F68. Weak negative charges of ~−18 mV were observed for atazanavir-loaded SLNs (Table I). The negative charge could be due to ionization of the stearic acid molecule (33).

Drug Release

The cumulative percent release of atazanavir from SLNs was evaluated over a 24 h time period, using PBS (10 mM, pH 7.4, 37°C) as the release medium. Atazanavir release from SLNs demonstrated an initial burst release of approximately 17% by 1 h with a gradual release up to 40% after 24 h (Fig. 2).

Cell Viability

The viability of hCMEC/D3 cells in the presence of either free atazanavir, blank SLNs or atazanavir-loaded SLNs was evaluated using a standard MTT assay. Cell viability was calculated as percent of control cells. The free aqueous atazanavir and surfactant (Pluronic® F68) solution showed little or no reduction in cell viability over a wide concentration range. The cell viability (Fig. 3) was approximately 100% for blank and atazanavir-loaded SLNs at a concentration corresponding to 200 nM of free atazanavir (corresponding to 3.21 μg/ml of stearic acid). Increasing the concentration of blank SLNs and atazanavir-loaded SLNs to 500 nM (corresponding to ~8.03 μg/ml of stearic acid) dropped the cell viability to approximately 60%. Exposure to varying concentrations of surfactant (Pluronic® F68) solution showed little or no reduction in cell viability.

Comparison of the Cellular Uptake of Atazanavir in Various Formulations

hCMEC monolayer cells were treated with (1) [^{3}H]-atazanavir-loaded SLNs, (2) blank SLNs in the presence of [^{3}H]-atazanavir aqueous solution or (3) [^{3}H]-atazanavir aqueous solution (all treatments were equivalent to 200 nM of free atazanavir). As seen in Fig. 4, there is no significant difference in the uptake of atazanavir when delivered by the three formulations at the early time points up to 60 min; however, there is a significant difference in atazanavir accumulated ($p<0.05$) by the cells treated with SLN encapsulated drug and the other two treatments at 120 min.

Imaging of Cellular Uptake of Rhodamine 123 Loaded SLNS using Fluorescence Microscopy

Rhodamine 123 (R123), a mitochondrial dye (34) was used as a hydrophobic fluorescence probe to compare uptake of R123 loaded SLNs to the uptake of an aqueous solution of R123. Fig. 5 shows fluorescence microscopy images of hCMEC/D3 monolayer cells exposed to R123 at 37°C for 2 h. The result strongly supports our quantitative measurements of the cellular uptake of [^{3}H]-atazanavir- loaded SLNs. R123 delivered by SLNs shows strong fluorescence in the cell cytoplasm. Little or no fluorescence can be detected from the control cells (treated with an aqueous solution of R123).

DISCUSSION

Atazanavir was efficiently extracted using methanol. The absorbance of the extracted atazanavir at 249 and 281 nm are in agreement with the standard sample at equivalent concentrations of 50 μg/ml (data not shown). A maximum of

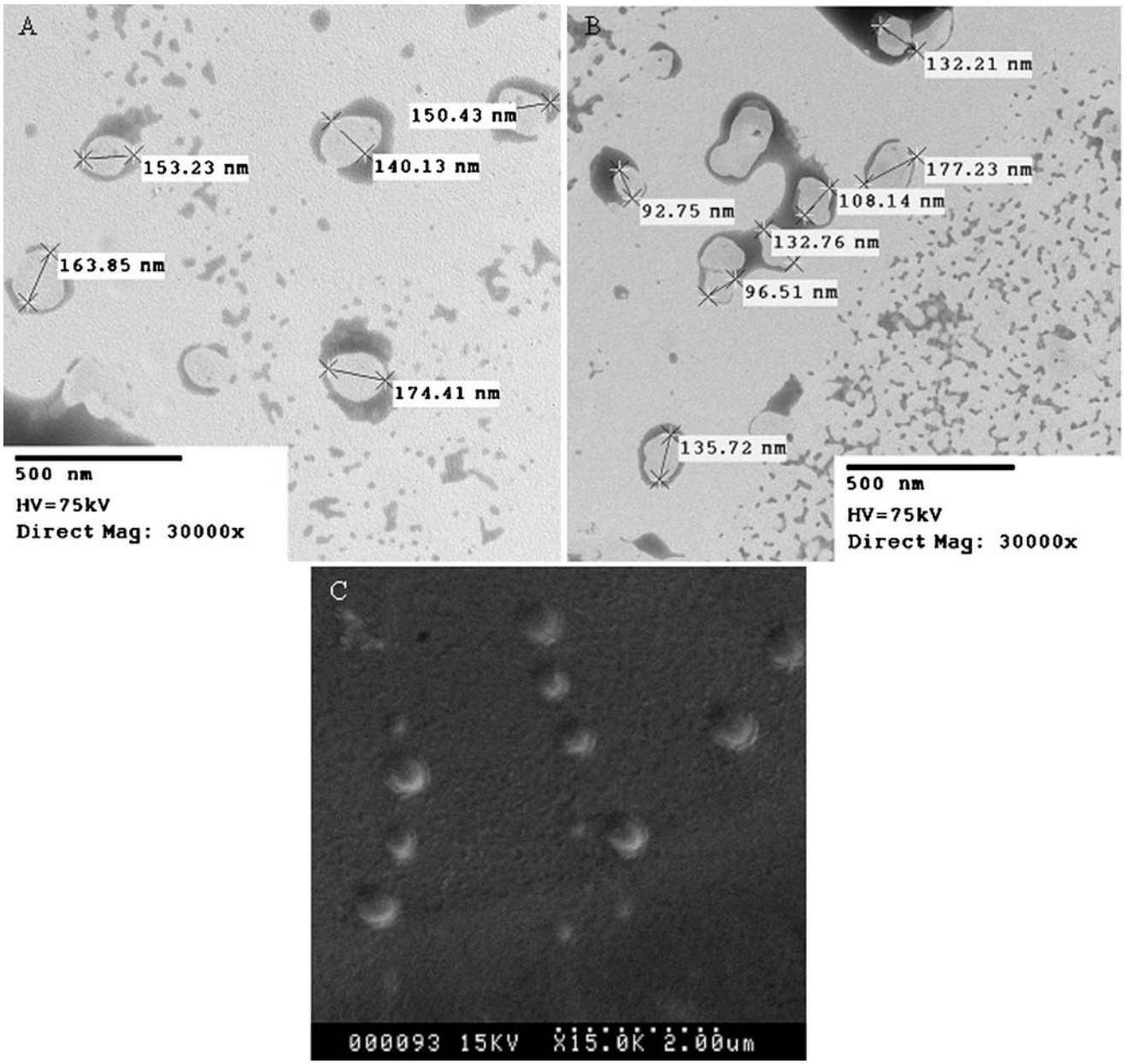

Fig. 1. Transmission electron microscopy of **A** blank stearic acid SLNs and **B** atazanavir loaded stearic acid SLNs. Particles were imaged using an accelerating voltage of 75 kV (magnification: ×30,000). **C** Scanning electron microscope image of atazanavir loaded stearic acid SLNs.

5% *w*/*w* loading could be achieved for atazanavir in stearic acid SLNs. Attempts to load atazanavir at a concentration higher than 5% *w*/*w* resulted in unstable formulations. Several key observations were made when drug loading higher than 5% *w*/*w* was attempted. For the 7.5% *w*/*w* load, the time to obtain a microemulsion was prolonged by several min and required an additional 10 min of sonication to obtain a clear phase. The formulation, however, precipitated on cooling. For the highest attempted loads (i.e., 10 and 20% *w*/*w*) a microemulsion was not obtained even with prolonged sonication and mechanical agitation. The instability could be attributed, in part, to a low concentration of emulsifier. A higher drug load for atazanavir may be achieved by utilizing different lipids in combination with more sophisticated manufacturing equipment such as high pressure homogenizers. The encapsulation efficiency results of atazanavir determined using [^{3}H]-atazanavir as tracer was in agreement with those obtained by UV spectrophotometry. On the contrary, it was found that R123 could only be loaded at relatively low loading amounts and the encapsulation efficiency was considerably lower to that obtained for atazanavir. Atazanavir, like other PIs, has a high lipophilicity, which could, in part, explain its high encapsulation in the lipid core and shell of the SLNs.

TEM images of blank SLNs and atazanavir-loaded SLNs illustrate nanoparticles with an average diameter of 156 nm which is in agreement to the particle size data obtained by dynamic light scattering. TEM analysis indicated a slight increase in particle size when the SLNs were loaded with atazanavir. SEM images confirm the formation of spherical nanoparticles with a smooth surface.

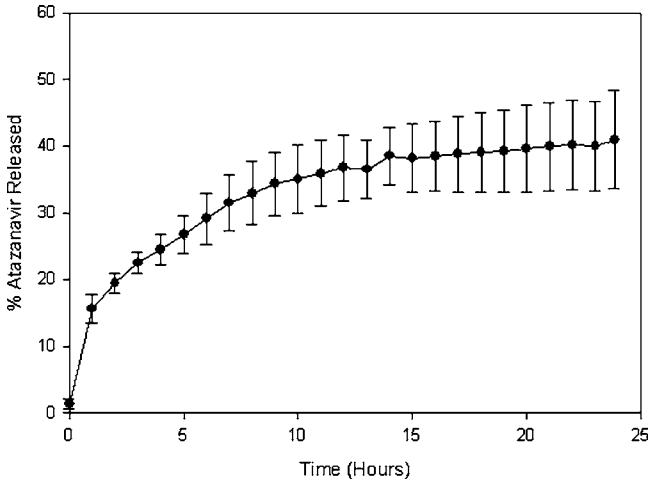

Fig. 2. Atazanavir release from stearic acid SLNs using PBS (10 mM, pH 7.4, 37°C) as the release medium(results are expressed as mean ± SD of three separate experiments).

We monitored the increase in particle size over one week for samples stored at 4°C as nanoparticles are prone to particle size growth during the ripening process (35), wherein a particle population continues to equilibrate *via* growth processes (36). In the first growth mechanism, known as Ostwald ripening, larger particles grow at the expense of those with smaller, less stable dimensions. In the second growth mechanism, known as Smoluchowski ripening, particles grow by coalescence through convection or active mixing (36). For SLNs it has been proposed that larger oil droplets can grow at the expense of smaller droplets, followed by possible droplet flocculation, droplet coalescence, and finally, phase separation (37). The size distribution of the particles is represented by the polydispersity index and a smaller value for the polydispersity index indicates that the particles have a smaller distribution range, which is critical for regulatory purposes. The nanoparticles formulated as per the microemulsion technique should ideally yield particles having an average diameter between 50 and 800 nm, preferably between 100 and 400 nm and a polydispersity index of between 0.06 and 0.90, preferably between 0.10 and 0.70 (38). As shown in Table I, our formulation exhibits a particle size distribution that falls within the preferred distribution range.

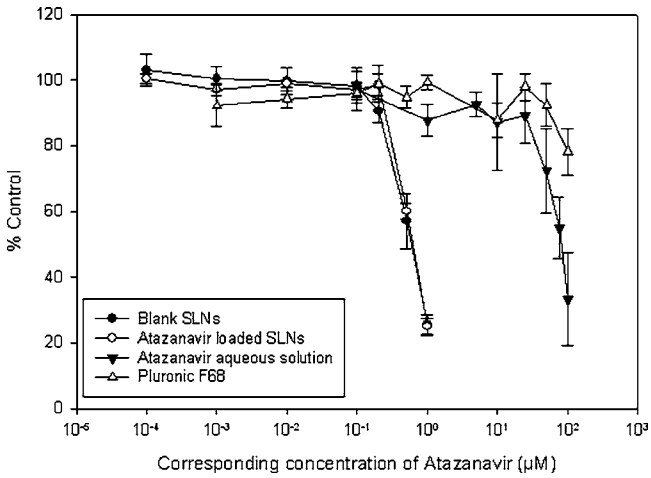

Fig. 3. Assessment of cell viability in the presence of atazanavir loaded SLNs, blank SLNs, surfactant and free atazanavir corresponding to varying concentrations of atazanavir (0.0001 to 100 μM), by a standard MTT assay. Results are expressed as mean±SEM of three separate experiments. In an individual experiment each experimental point was repeated six times.

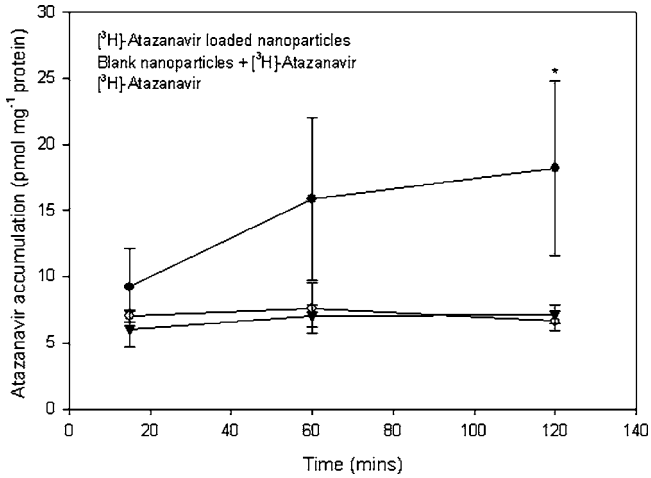

Fig. 4. Comparison of the cellular uptake of three treatments (1) [3H]-atazanavir loaded SLNs, (2) blank nanoparticles in the presence of [3H]-atazanavir aqueous solution and (3) [3H]-atazanavir aqueous solution by hCMEC/D3 monolayer cells. Results are expressed as mean±SD of three separate experiments. Asterisk represents data points that are significantly different from control (*$p<0.05$).

Atazanavir release from SLNs, as assessed using a dialysis bag technique, demonstrated an initial burst release of approximately 17% by 1 h with a gradual release up to 46% after 24 h. Since stearic acid is very slightly soluble in water (28), drug release due to dissolution of the stearic acid matrix in the release buffer is unlikely. For the slow and

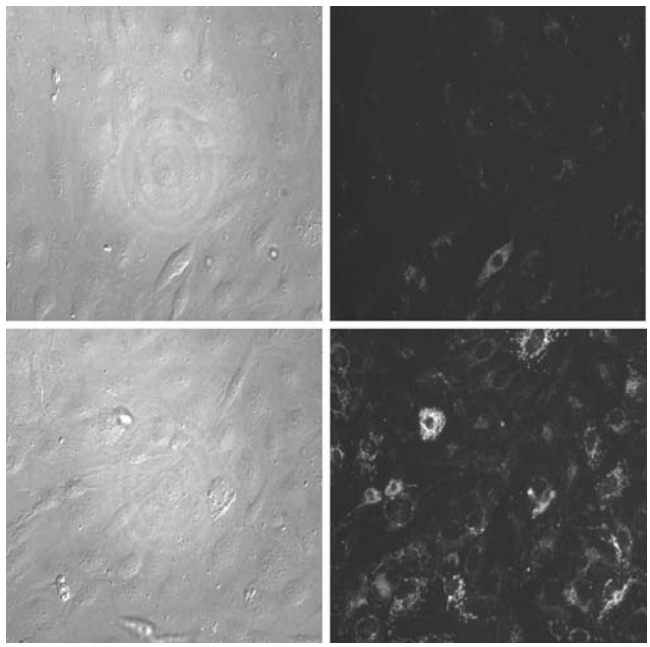

Fig. 5. Fluorescence microscopy images demonstrating the effect of R123 uptake by hCMEC/D3 cells. Differential interference contrast (DIC, *left panel*) and fluorescence images (*right panel*) of *top row*; Free R123 and *bottom row*; R123-loaded SLNs, after a 2 h incubation period (magnification: ×40).

incomplete release (~40%) seen at the end of a 24 h period it may be argued that the membrane enclosing the nanoparticles may be offering a diffusion barrier. However during the release experiments strict sink conditions were maintained and the drug concentration within the membrane would be higher than the concentration of drug outside the membrane resulting in a concentration gradient for the drug to diffuse out. It is known that lipids are prone to polymorphic transitions (39,40) and it is possible that there may have been polymorphic changes during the time course of the drug release study in the lipid structure that could delay drug release from the lipid nanoparticles.

The slow release of atazanavir from the matrix may be critical for delivery to the brain. Based on the hypothesis that endocytosis may be a major route of nanoparticle uptake by brain endothelial cells (41), an ideal formulation should have sustained delivery such that the encapsulated drug will not be released completely before the endocytotic process at the BBB takes place. The drug from the nanoparticles may then be released either within these cells followed by passive diffusion into the brain or can be transported into the brain by transcytosis (23).

The cytotoxicity of lipid nanoparticles in the human brain endothelial cell line (hCMEC/D3) was determined using a standard MTT assay and while atazanavir and Pluronic®F68 aqueous solution showed minimal toxicity over a wide concentration range, atazanavir loaded and blank SLNs demonstrated toxicity at concentrations corresponding to greater than 200 nM of aqueous atazanavir. Although the toxicity could be a major limiting factor in the full scale development of this formulation, atazanavir is a potent protease inhibitor with an EC50 of 2.6–5.3 nM and therefore for the therapeutic rationale of this study we are still capable of delivering approximately 50 times the EC50 dose *in vitro*.

Data on nanoparticle mediated toxicity is highly controversial. While some groups have reported that nanoparticles can exert cytotoxic effects in bovine brain microvessel endothelial cells (42,43), Lockman *et al.* (44) demonstrated that in the presence of emulsifying wax SLNs, no overall significant differences were observed *in vivo* for the cerebral perfusion flow. Furthermore, these authors reported that no statistically significant changes in barrier integrity, membrane permeability, or facilitated choline transport occurred *in vitro* in bovine brain microvessel endothelial cells. While the exact mechanism of nanoparticle mediated toxicity at the BBB is not clearly elucidated, there is some evidence that nanoparticle surface charge in terms of BBB targeting holds additional importance. Lockman *et al.* (45) reported that neutral nanoparticles (−14.1 mV) and low concentrations of anionic nanoparticles (−59.5 mV) did not exert any effect on BBB integrity, whereas high concentrations of anionic NPs and cationic NPs disrupted the BBB. In addition, brain uptake rates of anionic NPs were found superior to neutral or cationic formulations when used at the same concentrations. The authors concluded that neutral and low concentrations of anionic NPs can be used safely as colloidal drug carriers to brain. In our studies, we observed only weak negative charges of ~−18 mV for atazanavir-loaded SLNs. Based on these reports, we suggest that the currently developed formulation with a weak negative charge of ~ −18 mV may not be exerting a surface charge mediated cytotoxic effect.

The influence of the lipid carrier on cytotoxicity depends on the cell line used (46). Our laboratory (47) has demonstrated that blank stearic acid SLNs have no toxicity towards human breast carcinoma cell lines, MDA-435/LCC6/MDR1 (overexpressing P-glycoprotein) and its parent cell line MDA-435/LCC6/WT at concentrations up to 200 μg/ml stearic acid SLNs. Muller *et al.* (48) studied the *in vitro* cytotoxicity of SLN lipid matrices (Dynasan 114 and Compritol ATO 888) using human promyelotic (HL60) cells and found no toxicity. Additionally, they demonstrated that these lipid matrices showed lower cytotoxicity compared to polyalkylcyanoacrylate and polylactic/glycolic acid (PLA/GA) nanoparticles. Carsten *et al.* (46) observed marked toxicity when cells were incubated with SLN consisting of stearic acid at concentrations of 0.01%, whereas SLN consisting of triglycerides, cetylpalmitate or paraffin did not exert major cytotoxic effects at the same concentrations. The authors suggest that the cytotoxic effects were most likely caused by products of enzymatic degradation including free stearic acid.

To the best of our knowledge, our group is the first to study the interactions of lipid nanoparticles with a well characterized human brain endothelial cell line. While the hCMEC/D3 cell line provides replicate cultures of cells for characterization and assay of specific parameters such as transport mechanisms, as with other cell lines, it could evolve away from the phenotype of the original transformed cell due to inherent genetic instability and selective adaptation to the culture environment (49). The presence of other cell types (i.e., astrocytes, oligodendrocytes) conditioning the cell microenvironment may influence the transport and metabolic properties of culture cells and possibly be required to mimic more closely the *in vivo* situation (49). Our cell viability experiments with blank SLNs indicate that the hCMEC/D3 cells are sensitive to stearic acid SLNs and possibly other lipid matrices, suggesting that lipids/polymers intended for BBB targeting could be screened for preliminary toxicity using this cell line. Lack of toxicity of lipid matrices to other cell lines such as HL60 may not be indicative of non toxicity to brain cells. In brief, such dramatic variations in cell line dependent toxicity suggest that according to the desired therapeutic application, lipid matrices for engineering SLNs should be carefully chosen and evaluated prior to *in vivo* testing.

Uptake studies using [^{3}H]-atazanavir demonstrate that there is a significantly higher uptake in the hCMEC/D3 cells when delivered by SLNs. Incubation of blank SLNs with an aqueous solution of [^{3}H]-atazanavir showed no increase in cellular uptake of [^{3}H]-atazanavir suggesting that atazanavir has to be associated with the nanoparticles in order to have increased cellular accumulation. This is in agreement with the reports of Kreuter *et al.* (50), which showed that in order for a drug to be efficiently delivered across the BBB it had to be physically associated with polymeric nanoparticles. The variability in atazanavir uptake when delivered by SLNs as observed in our experiments can be attributed, in part, to variations in particle size and drug loading as a result of the SLNs synthesis process. To further characterize cellular uptake of drug delivered by SLNs using the hCMEC/D3 cells we used R123, a mitochondrial fluorescent probe to visualize cellular uptake and localization by fluorescence microscopy. Fig. 5 makes evident that there is higher cellular uptake of R123 when delivered by SLNs as compared to an aqueous solution

of R123. Although there is a higher cell uptake of R123 when delivered by SLNs, there is no discernable difference in intracellular localization of the dye indicating that the SLNs may only be facilitating the uptake of R123. Upon cell uptake, R123 could be released from the particles allowing R123 to enter the mitochondria. Since R123 loaded SLNs are a colloidal system, the number of R123 encapsulated SLNs exposed to each cell will vary (due to Brownian motion as well as electrostatic interactions). Thus, certain cells seem to take up higher amounts of R123 delivered by SLNs which can be attributed to the amount of SLNs and differential expression of cell surface receptors as well as transporters. It should be noted that both atazanavir (51) and R123 (52) are substrates of ATP-binding cassette membrane-associated drug efflux transporters such as P-gp and their intracellular drug concentration can be reduced by the activity of these transporters (53,54). It has been previously demonstrated (55) that nanoparticles can circumvent P-gp mediated efflux and increase intracellular accumulation of pharmacological agents. Therefore, it may be possible that the atazanavir and R123 loaded SLNs could bypass the membrane bound P-gp efflux pump or mask the encapsulated drug from P-gp recognition (56) thereby increasing their intracellular accumulation. In conclusion, our fluorescence microscopy images further support and suggest enhanced intracellular accumulation of atazanavir in human brain endothelial cells *in vitro* through use of SLN delivery system.

CONCLUSION

SLNs with a high encapsulation of the potent HIV PI, atazanavir (≥90%) were successfully prepared and characterized. Results from cell viability studies coupled with higher drug cellular uptake suggest that SLNs can effectively deliver atazanavir to human brain endothelial cells, *in vitro*. Future drug uptake studies in an *in vivo* model will demonstrate the potential efficacy of SLNs to deliver atazanavir to the brain.

ACKNOWLEDGMENTS

This research is supported by a grant from the Ontario HIV Treatment Network awarded to Dr. R. Bendayan. The authors thank Mr. K. Babakhanian, Mr. B. Calvieri and Mr. S. Doyle for technical assistance with fluorescence and electron microscopy imaging.

REFERENCES

1. S. Swindells. Current concepts in the treatment of HIV infection with focus on brain disease. In I. G. H. E. Gendelman, I. P. Everall, S. A. Lipton, and S. Swindells (eds.), *The Neurology of AIDS*, Oxford University Press, New York, 2005.
2. F. Aweeka, A. Jayewardene, S. Staprans, S. E. Bellibas, B. Kearney, P. Lizak, T. Novakovic-Agopian, and R. W. Price. Failure to detect nelfinavir in the cerebrospinal fluid of HIV-1-infected patients with and without AIDS dementia complex. *J. Acquir. Immune Defic. Syndr. Human Retrovirol.* **20**(1):39–43 (1999).
3. S. A. Thomas. Anti-HIV drug distribution to the central nervous system. *Curr. Pharm. Des.* **10**(12):1313–1324 (2004).
4. A. Schnyder, and J. Huwyler. Drug transport to brain with targeted liposomes. *NeuroRx*. **2**(1):99–107 (2005).
5. A. E. Gulyaev, S. E. Gelperina, I. N. Skidan, A. S. Antropov, G. Y. Kivman, and J. Kreuter. Significant transport of doxorubicin into the brain with polysorbate 80-coated nanoparticles. *Pharm. Res*. **16**(10):1564–1569 (1999).
6. J. Wang, X. Sun, and Z. Zhang. Enhanced brain targeting by synthesis of 3,5-dioctanoyl-5-fluor-2-deoxyuridine and incorporation into solid lipid nanoparticles. *Eur. J. Pharm. Biopharm.* **54**(3):285–290 (2002).
7. J. Kreuter. Nanoparticulate systems for brain delivery of drugs. *Adv. Drug Deliv. Rev*. **47**(1):65–81 (2001).
8. T. K. Vyas, L. Shah, and M. M. Amiji. Nanoparticulate drug carriers for delivery of HIV/AIDS therapy to viral reservoir sites. *Expert Opin. Drug Deliv*. **3**(5):613–628 (2006).
9. L. Kinman, T. Bui, K. Larsen, C- Tsai, D. Anderson, W. R. Morton, S- Hu, and R. J. Y. Ho. Optimization of lipid-indinavir complexes for localization in lymphoid tissues of HIV-infected macaques. *J. Acquired Immune Defic. Syndr.* **42**(2):155–161 (2006).
10. J. F. Gagne, A. Desormeaux, S. Perron, M. J. Tremblay, and M. G. Bergeron. Targeted delivery of indinavir to HIV-1 primary reservoirs with immunoliposomes. *Biochim. Biophys. Acta*. **1558**(2):198–210 (2002).
11. A. Deìsormeaux, and M. G. Bergeron. Lymphoid tissue targeting of anti-HIV drugs using liposomes. *Methods Enzymol*. **391**(SPEC. ISS.):330–351 (2005).
12. A. R. Bender, H. Von Briesen, J. Kreuter, I. B. Duncan, and H. Rubsamen-Waigmann. Efficiency of nanoparticles as a carrier system for antiviral agents in human immunodeficiency virus-infected human monocytes/macrophages *in vitro*. *Antimicrob. Agents Chemother.* **40**(6):1467–1471 (1996).
13. H. Dou, J. Morehead, C. J. Destache, J. D. Kingsley, L. Shlyakhtenko, Y. Zhou, M. Chaubal, J. Werling, J. Kipp, B. E. Rabinow, and H. E. Gendelman. Laboratory investigations for the morphologic, pharmacokinetic, and anti-retroviral properties of indinavir nanoparticles in human monocyte-derived macrophages. *Virology*. **358**(1):148–158 (2007).
14. L. K. Shah, and Mansoor M. Amiji. Intracellular delivery of saquinavir in biodegradable polymeric nanoparticles for HIV/AIDS. *Pharm. Res*. **23**(11):2638–2645 (2006).
15. R. Lobenberg, L. Araujo, and J. Kreuter. Body distribution of azidothymidine bound to nanoparticles after oral administration. *Eur. J. Pharm. Biopharm.* **44**(2):127–132 (1997).
16. R. Lobenberg, J. Maas, and J. Kreuter. Improved body distribution of 14C-labelled AZT bound to nanoparticles in rats determined by radioluminography. *J. Drug Target*. **5**(3):171–179 (1998).
17. Reddy L. Harivardhan, R. S. R. Murthy, R. K. Sharma, K. Chuttani, and A. K. Mishra. Influence of administration route on tumor uptake and biodistribution of etoposide loaded solid lipid nanoparticles in dalton's lymphoma tumor bearing mice. *J. Control. Release*. **105**(3):185–98 (2005).
18. G. P. Zara, R. Cavalli, A. Bargoni, A. Fundarò, D. Vighetto, and M. R. Gasco. Intravenous administration to rabbits of non-stealth and stealth doxorubicin-loaded solid lipid nanoparticles at increasing concentrations of stealth agent: Pharmacokinetics and distribution of doxorubicin in brain and other tissues. *J. Drug Target*. **10**(4):327–335 (2002).
19. A. Fundaro, R. Cavalli, A. Bargoni, D. Vighetto, G. P. Zara, and M. R. Gasco. Non-stealth and stealth solid lipid nanoparticles (SLN) carrying doxorubicin: Pharmacokinetics and tissue distribution after i.v. administration to rats. *Pharmacol. Res*. **42**(4):337–343 (2000).
20. A. Bargoni, R. Cavalli, O. Caputo, A. Fundarò, M. R. Gasco, and G. P. Zara. Solid lipid nanoparticles in lymph and plasma after duodenal administration to rats. *Pharm. Res*. **15**(5):745–750 (1998).
21. J. M. Koziara, R. J. Mumper, J. J. Oh, W. S. Akers, and S. P. Ferraris. Blood compatibility of cetyl alcohol/polysorbate-based nanoparticles. *Pharm. Res*. **22**(11):1821–1828 (2005).
22. P. R. Lockman, M. O. Oyewumi, J. M. Koziara, K. E. Roder, R. J. Mumper, and D. D. Allen. Brain uptake of thiamine-coated nanoparticles. *J. Control. Release*. **93**(3):271–282 (2003).
23. J. Kreuter. Influence of the surface properties on nanoparticle-mediated transport of drugs to the brain. *J Nanosci Nanotechnol*. **4**(5):484–488 (2004).
24. H. R. Kim, S. Gil, K. Andrieux, V. Nicolas, M. Appel, H. Chacun, D. Desmaele, F. Taran, D. Georgin, and P. Couvreur.

Low-density lipoprotein receptor-mediated endocytosis of PEGylated nanoparticles in rat brain endothelial cells. *Cell. Mol. Life Sci*. **64**(3):356–364 (2007).
25. Y- Gong, B. Robinson, R. Rose, C. Deminie, T. Spicer, and M. Markowitz. Antiviral activity and resistance profile of an HIV-1 protease inhibitor BMS-232632. 38th Interscience Conference on Antimicrobial Agents and Chemotherapy, 1998.
26. X. Rabasseda, J. Silvestre, and J. Castañer. BMS-232632. Anti-HIV, HIV-1 protease inhibitor. *Drugs Future*. **24**(4):375–380 (1999).
27. R. W. Sparidans, F. Dost, K. M. Crommentuyn, A. D. Huitema, J. H. Schellens, and J. H. Beijnen. Liquid chromatographic assay for the protease inhibitor atazanavir in plasma. *Biomed. Chromatogr.* **20**(1):72–76 (2006).
28. Susan Budavari, and Maryadele J. O'Neil. The Merck index: an encyclopedia of chemicals, drugs, and biologicals, 13th edn, Merck, Whitehouse Station, NJ, 2001.
29. D. Aquilano, R. Cavalli, and M. R. Gasco. Solid lipospheres obtained from hot microemulsions in the presence of different concentrations of cosurfactant: The crystallization of stearic acid polymorphs. *Thermochim. Acta.* **230**:29–37 (1993).
30. H. Komatsu, A. Kitajima, and S. Okada. Pharmaceutical characterization of commercially available intravenous fat emulsions: Estimation of average particle size, size distribution and surface potential using photon correlation spectroscopy. *Chem. Pharm. Bull.* (Tokyo). **43**(8):1412–1415 (1995).
31. J. Carmichael, W. Degraff, A. Gazdar, J. Minna, and J. Mitchell. Evaluation of a tetrazolinum-based semiautomated colorimetric assay: Assessment of chemosensitivity testing. *Cancer Res.* **47**:936–942 (1978).
32. P. T. Ronaldson, and R. Bendayan. HIV-1 viral envelope glycoprotein gp120 triggers an inflammatory response in cultured rat astrocytes and regulates the functional expression of P-glycoprotein. *Mol. Pharmacol*. **70**(3):1087–1098 (2006).
33. H. L. Wong, R. Bendayan, A. M. Rauth, and X. Y. Wu. Development of solid lipid nanoparticles containing ionically complexed chemotherapeutic drugs and chemosensitizers. *J Pharm. Sci*. **93**(8):1993–2008 (2004).
34. L. V. Johnson, M. L. Walsh, and L. B. Chen. Localization of mitochondria in living cells with rhodamine 123. *Proc. Natl. Acad Sci*. **77**(2):990–994 (1980).
35. M. Wei, A. J. Ruys, B. K. Milthorpe, and C. C. Sorrell. Solution ripening of hydroxyapatite nanoparticles: Effects on electrophoretic deposition. *J. Biomed. Materi. Res.* **45**(1):11–19 (1999).
36. A. J. Barker, B. Cage, S. Russek, and C. R. Stoldt. Ripening during magnetite nanoparticle synthesis, Resulting interfacial defects and magnetic properties. *J. Appl. Phys.* **98**(6):1–7 (2005).
37. D. Michael. Triplett II. Enabling Solid Lipid Nanoparticle Drug Delivery Technology By Investigating Improved Production Techniques. [Doctor of Philosophy]. The Ohio State University: The Ohio State University; 2004 Available from: The Ohio State University.
38. Maria R. Gasco, Lungo Po Antonelli. Method for preparing solid lipid microspheres having a narrow size distribution. USA patent 5,250,236. 1993.
39. W. Sutananta, D. Q. Craig, and J. M. Newton. An investigation into the effects of preparation conditions and storage on the rate of drug release from pharmaceutical glyceride bases. *J. Pharm. Pharmacol*. **47**(5):355–359 (1995).
40. J. Hamdani, A. J. Moes, and K. Amighi. Development and evaluation of prolonged release pellets obtained by the melt pelletization process. *Int. J. Pharm*. **245**(1–2):167–177 (2002).
41. R. N. Alyaudtin, A. Reichiel, R. Lobenberg, P. Ramge, J. Kreuter, and D. J. Begley. Interaction of poly(butylcyanoacrylate) nanoparticles with the blood-brain barrier *in vivo* and *in vitro*. *J. Drug Target*. **9**(3):209–221 (2001).
42. J. Olivier, L. Fenart, R. Chauvet, C. Pariat, R. Cecchelli, and W. Couet. Indirect evidence that drug brain targeting using polysorbate 80- coated polybutylcyanoacrylate nanoparticles is related to toxicity. *Pharm. Res*. **16**(12):1836–1842 (1999).
43. S. Steiniger, D. Zenker, H. V. Briesen, D. Begley, and J. Kreuter. The influence of polysorbate 80-coated nanoparticles on bovine brain capillary endothelial cells *in vitro*. *Proc. Int. Symp. Control Rel. Bioact. Mater.* **26**:789–790 (1999).
44. P. R. Lockman, J. Koziara, K. E. Roder, J. Paulson, T. J. Abbruscato, R. J. Mumper, and D. D. Allen. *In vivo* and *in vitro* assessment of baseline blood-brain barrier parameters in the presence of novel nanoparticles. *Pharm. Res*. **20**(5):705–713 (2003).
45. P. R. Lockman, D. Allen, J. M. Koziara, and R. J. Mumper. Nanoparticle surface charges alter blood-brain barrier integrity and permeability. *J. Drug Target*. **12**(9–10):635–641 (2004).
46. Carsten Olbrich, Kerstin Tabatt, Sylvia A. Wissing, Nadja Schöler, and R. H. Müller. Solid lipid nanoparticles (SLN): interaction with cells, cytokine production and enzymatic degradation. In C. Nastruzzi (ed.), *Lipospheres in Drug Targets and Delivery: Approaches, Methods, and Applications*, 1st edn. 2005.
47. H. L. Wong, A. M. Rauth, R. Bendayan, J. L. Manias, M. Ramaswamy, Z. Liu, S. Z. Erhan, and X. Y. Wu. A new polymer-lipid hybrid nanoparticle system increases cytotoxicity of doxorubicin against multidrug-resistant human breast cancer cells. *Pharm. Res*. **23**(7):1574–1585 (2006).
48. R. H. Müller, D. Rühl, S. Runge, W. Mehnert, and K. Schulze-Forster. Cytotoxicity of solid lipid nanoparticles as a function of the lipid matrix and the surfactant. *Pharm. Res*. **14**(4):458–462 (1997).
49. M. Hong. Transport properties of thymidine and it analog, Zidovudine (ZDV) by microglia cells: Relevance to HIV-1 encephalopathy and AIDs dementia. M.Sc. University of Toronto; 2001 p.
50. J. Kreuter, P. Ramge, V. Petrov, S. Hamm, S. E. Gelperina, B. Engelhardt, R. Alyautdin, H. von Briesen, and D. J. Begley. Direct evidence that polysorbate-80-coated poly(butylcyanoacrylate) nanoparticles deliver drugs to the CNS via specific mechanisms requiring prior binding of drug to the nanoparticles. *Pharm. Res*. **20**(3):409–416 (2003).
51. M. B. Lucia, S. Rutella, E. Rastrelli, A. Savarino, R. Cauda, and C. Golotta. Atazanavir inhibits P-glycoprotein and multidrug resistance-associated protein efflux activity. *J. Acquir. Immune Defic. Syndr.* **39**(5):635–637 (2005).
52. J. S. Lee, K. Paull, M. Alvarez, C. Hose, A. Monks, M. Grever, A. T. Fojo, and S. E. Bates. Rhodamine efflux patterns predict P-glycoprotein substrates in the national cancer institute drug screen. *Mol. Pharmacol.* **46**(4):627–638 (1999).
53. R. Bendayan, P. T. Ronaldson, D. Gingras, and M. Bendayan. *In situ* localization of P-glycoprotein (ABCB1) in human and rat brain. *J. Histochem. Cytochem.* **54**(10):1159–1167 (2006).
54. C. Cordon-Cardo, J. P. O'Brien, D. Casals, L. Rittman-Grauer, J. L. Biedler, M. R. Melamed, and J. R. Bertino. Multidrug-resistance gene (P-glycoprotein) is expressed by endothelial cells at blood–brain barrier sites. *Proc. Natl. Acad. Sci U.S.A*. **86**(2):695–698 (1989).
55. H. L. Wong, R. Bendayan, A. M. Rauth, H. Y. Xue, K. Babakhanian, and X. Y. Wu. A mechanistic study of enhanced doxorubicin uptake and retention in multidrug resistant breast cancer cells using a polymer-lipid hybrid nanoparticle system. *J. Pharmacol. Exp. Ther.* **317**(3):1372–1381 (2006).
56. J. M. Koziara, P. R. Lockman, D. D. Allen, and R. J. Mumper. Paclitaxel nanoparticles for the potential treatment of brain tumors. *J. Control Release*. **30**;99(2):259–269 (2004).